IEEE Access
Multidisciplinary | Rapid Review | Open Access Journal

Received March 2, 2021, accepted March 15, 2021, date of publication March 18, 2021, date of current version March 29, 2021.

Digital Object Identifier 10.1109/ACCESS.2021.3067023

Mid-Range Wireless Power Transfer System for Various Types of Multiple Receivers Using Power Customized Resonator

HANSIK OH, SUNGJAE OH, HYUNGMO KOO, WOOJIN CHOI, JAEKYUNG SHIN, KEUM CHEOL HWANG, (Senior Member, IEEE), KANG-YOON LEE, (Senior Member, IEEE), AND YOUNGOO YANG, (Senior Member, IEEE)

Department of Electrical and Computer Engineering, Sungkyunkwan University, Suwon 16419, South Korea

Corresponding author: Youngoo Yang (yang09@skku.edu)

This work was supported by the National Research Foundation of Korea (NRF) Grant by the Korean government through MSIP under Grant 2018R1A2B3005479.

ABSTRACT This paper presents a high-efficiency wireless power transfer (WPT) system that can charge multiple receivers (Rx's) of various types. For system analysis, the transmitted power and received power levels are derived using the parameters of the resonators based on electro-magnetic (EM) resonance. Using the analysis results, the power customized resonator (PCR) not only for deriving sufficient output power from the transmitter (Tx) but also for appropriately distributing the received power to the various and multiple Rx's is proposed. In addition to the PCR, the Tx unit is designed to work as a load-dependent voltage source using a differential Class-E power amplifier (PA) through a wide range of load impedances. Therefore, the Tx can naturally adapt to the required Tx power levels with a high efficiency corresponding to various Rx configurations without additional tunable circuits or adaptive control schemes. The WPT system, including the load-dependent voltage source for the Tx, full-bridge rectifiers for the Rx's, and the proposed PCR, was designed for the 6.78 MHz frequency band. The proposed system is validated for use with multiple mobile devices by conducting experiments with nine charging cases using three types of Rx's. For all cases, high system efficiencies of 70.7-85.5% were maintained over received power levels of 8.6-45.7 W at a charging distance of 30 mm, and each of the three types of Rx's were experimentally verified to receive sufficient power.

INDEX TERMS Wireless power transfer, multiple-receiver charging, electromagnetic resonance, power customized resonator, Class-E power amplifier.

I. INTRODUCTION

Recently wireless power transfer (WPT) has emerged as a great alternative to charge mobile or wearable devices. User convenience increases when power cables are removed from devices to wirelessly transfer power, but a challenging issue is to charge multiple devices simultaneously using one Tx. The ability to simultaneously charge multiple Rx's using one Tx will result in a wireless charging system that is more effective and convenient. In particular, charging methods for multiple Rx's can be suitable for use in a variety of public spaces, such as airports, cafeterias, libraries, and offices, as well as for the home.

The associate editor coordinating the review of this manuscript and approving it for publication was Tae Wook Kim.

In addition to industrial developments, many academic studies have been conducted on Tx, Rx, and coupled resonators for advanced WPT technologies [1]–[32]. A coupled resonator, a core block of WPT systems, uses EM resonance to transfer power from the Tx to the Rx without a physical connection between them. In [1]–[7], the materials and structure of the coupled resonator were discussed to have a low loss. In [4]–[6], the power distribution for multiple Rx coils that are coupled with one Tx coil was derived from an equivalent circuit of the resonator. In [4], an impedance matching network was proposed to convert the load impedance at the Rx to control the power division ratio for multiple Rx coils. Using the impedance inverter, the power division ratio was generalized for an arbitrary number of Rx's. The measured S-parameters for the resonators with one Tx coil and two Rx

This work is licensed under a Creative Commons Attribution 4.0 License. For more information, see https://creativecommons.org/licenses/by/4.0/

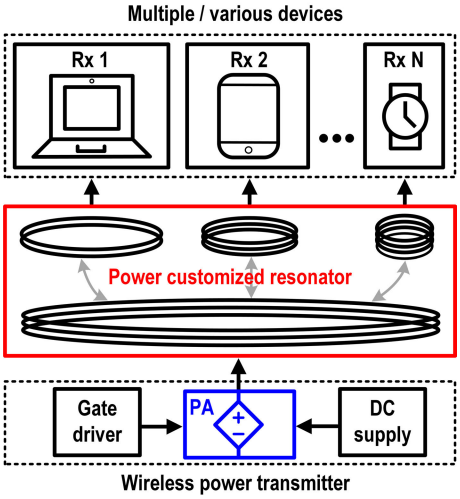

FIGURE 1. WPT system for multiple charging using three different types of Rx's.

coils were presented at a frequency of 13.56 MHz. In [5], the optimum Rx load impedance was derived for maximum efficiency using an equivalent circuit model of the resonator including multiple Rx coils. Using three different Rx coils, efficiency of the resonator of above 80% was presented under the optimal load condition. Reference [6] analyzed the input impedance and power division ratio of the resonator, including a cross-coupling effect between the Rx coils. The compensation using an optimum load reactance was shown to recover the degradation in efficiency and shift in resonant frequency due to cross-coupling. However, since these previous studies have focused only on a resonator, the system-level operation cannot be optimized including the PA at Tx and the rectifier at Rx. The resonator for multiple Rx coils must be co-analyzed and co-designed with the Tx and Rx circuits.

Several WPT systems including the Tx, Rx, and coupled resonator were presented in [8]–[31]. Especially in [19]–[21], WPT systems to charge multiple Rx's were designed and verified at the 6.78 MHz frequency band. Reference [19] used the adaptive closed-loop duty cycle control of the buck converter to report an average system efficiency of 71.7% maintained for the three Rx's. In [20], a class-E PA was designed to provide a robust operation for varying load conditions according to the random battery voltage distribution, and it exhibited a system efficiency of 71.0% for six Rx's. However, a fixed number of homogeneous multiple Rx's was dealt with in [19], [20]. In [21], the charging cases were extended, but the received power of each Rx was reduced, and the system efficiency became relatively low for cases with multiple charging. In addition, a control circuit using switches and a controller in the Tx can significantly increase the complexity of the system.

Fig. 1 shows a conceptual diagram of the proposed WPT system for various types of multiple Rx's. The proposed WPT system can charge various types of mobile devices, such as a laptop, tablet, cell phone, and wearable device, at the same time. Multiple Rx's are configured with different physical sizes and power demand. To charge a single Rx, the Tx should generate the appropriate power with a high efficiency for the power demand, which varies according to the type of Rx. To charge multiple Rx's in either homogeneous or heterogeneous configurations, the Tx should generate the appropriate power with a high efficiency, which is the sum of the power demand from multiple Rx's. In addition, the power generated from the Tx should be accurately distributed to each Rx according to the power demand of each Rx.

In this paper, a high-efficiency WPT system having capability of charging various types of multiple Rx's is presented. Through the analysis using an equivalent circuit of the resonator including the Tx coil and multiple Rx coils, the transmitted and received power was derived using parameters of the resonator. The input impedance of the PCR is designed to be proportional to the required transmitted power for any of the Rx configurations. Based on the analysis results, we proposed the PCR not only to derive a sufficient power from the Tx but also to appropriately distribute the transmitted power to each of the multiple Rx's according to the power demand. Compared to the resonators in [1]–[7], the proposed PCR has a unique feature for the WPT systems to fulfill the power demands of the various multiple Rx's that are matched to the same reference impedance.

For the Tx, a load-dependent voltage source to generate the power required for the PCR was designed based on a differential Class-E PA with a simple L-C impedance transformation network (ITN). Over a wide impedance range, the proposed load-dependent voltage source as the Tx can generate an output power proportional to the load impedance (i.e. input impedance of the PCR) with a high efficiency. The PCR should be designed to have the input impedance that is proportional to the required transmitted power. Therefore, the proposed Tx based on a load-dependent voltage source can supply the appropriate amount of power to multiple Rx's in various configurations through the PCR without any tunable or adaptive circuit.

The Tx based on the load-dependent voltage source, various types of multiple Rx's, and the proposed PCR were co-designed and implemented to achieve the optimum operation of the WPT system to charge multiple devices. Nine charging cases using three different Rx's were selected to experimentally verify the proposed PCR and load-dependent voltage source. For all selected cases, the overall system efficiency and the received power are presented and compared to those from previously published works.

II. ANALYSIS OF THE WPT SYSTEM FOR CHARGING VARIOUS TYPES OF THE MULTIPLE RX's

A. LOAD-DEPENDENT VOLTAGE SOURCE USING A CLASS-E PA

Class-E PA having theoretical efficiency of 100% converts the input dc power to the power of the radio-frequency (RF) signal. Class-E PAs can be designed using a switch and lumped components with a high quality-factor to achieve a high efficiency. For classical approaches, accurate operation

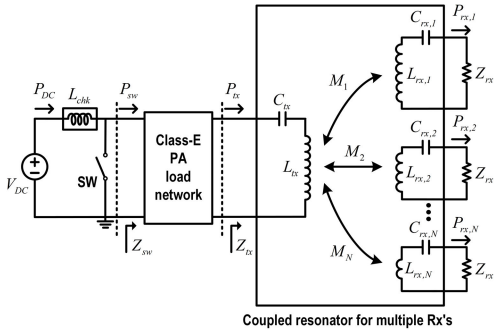

FIGURE 2. Diagram of the WPT system to charge various types of multiple Rx's.

has been achieved by adding an inductive element at a fixed resistive load [32]–[33]. To achieve a higher output power, an impedance matching network based on an L-C or C-L-C network can be used to provide the optimum load impedance to the switch. However, for general WPT systems, the load impedance of the Tx (or input impedance of the resonator) varies widely according to the number of Rx's, the overall power demand from the Rx's, and the coupling coefficient between the Tx and Rx coils of the resonator, which should be carefully considered when designing the PA.

For analysis, a simplified equivalent network of the WPT system for charging various types of multiple Rx's, as shown in Fig. 2. It will be assumed that the Class-E PA is ideal and the coils in the resonator are lossless in the analysis. Class-E PA consists of a switch and a load network including a conventional shunt capacitor, a series L-C resonant network and an additional matching network for impedance transformation. L_{chk} is an ideal RF chock, and V_{DC} is the supply voltage of the Class-E PA. N is the number of Rx's, and M_i is the mutual inductance between the Tx and i-th Rx coils in the resonator. L_{tx} and $L_{rx,i}$ are the self-inductance of the Tx and i-th Rx coils, respectively. C_{tx} and $C_{rx,i}$ have resonance with L_{tx} and $L_{rx,i}$, respectively, as follows.

$$j\omega_0 L_{tx} + \frac{1}{j\omega_0 C_{tx}} = 0, \tag{1}$$

$$j\omega_0 L_{rx,i} + \frac{1}{j\omega_0 C_{rx,i}} = 0, \tag{2}$$

where Ω_0 is the operation frequency of the system. Z_{tx}, Z_{rx}, and Z_{sw} are the load impedances of the Tx, Rx, and switch, respectively. P_{DC}, P_{tx}, and $P_{rx,i}$ are the input DC power of the PA, the output RF power of the Tx, and the received power of the i-th Rx. P_{rx} is a sum of the received power from N Rx's, which is expressed as follows.

$$P_{rx} = \sum_{i=1}^{N} P_{rx,i}. \tag{3}$$

Since an ideal Class-E PA and a lossless resonator were assumed,

$$P_{DC} = P_{rx} = P_{tx}. \tag{4}$$

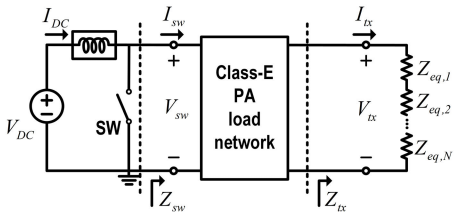

FIGURE 3. Schematic diagram of the WPT Tx using equivalent impedances for multiple Rx's.

Using the equivalent circuit model for the resonator, the impedances looking toward the resonator from the Tx output were derived in previous works [4], [5]. Fig. 3 shows a schematic diagram of the WPT system using equivalent impedances for multiple Rx's. I_{DC} is the dc supply current of the PA. V_{sw} and V_{tx} are the fundamental voltages of the switch and of the Tx load, respectively. I_{sw} and I_{tx} are the fundamental currents from the switch and from the Tx output, respectively. The equivalent impedance of i-th Rx, $Z_{eq,i}$, becomes as follows.

$$Z_{eq,i} = \frac{\omega_0^2 M_i^2}{Z_{rx}}. \tag{5}$$

Then, the load impedance of the Tx (Z_{tx}) becomes a sum of N equivalent Rx impedances, which can be represented as follows.

$$Z_{tx} = \frac{\omega_0^2}{Z_{rx}} \sum_{i=1}^{N} M_i^2. \tag{6}$$

From (6), Z_{tx} becomes a pure real value (i.e. resistance) if Z_{rx} is a pure real value. This also indicates that the load impedance of the Tx (Z_{tx}) increases as the number of Rx's (N) increases. Accordingly, the output power of the Tx should be increased to satisfy the increased power demand of the increased number of Rx's which is proportional to Z_{tx}.

The Tx can be regarded as a power source that generates the RF power and supplies the generated power to the resonator. The power amplifier in the output power saturation condition behaves as a current source at the internal plane of the transistor since the intrinsic transistor can be modeled as a voltage-controlled current source. The RF current of this current source is determined by the load resistance while the RF voltage is constant. Therefore, the power amplifier for this case can be simply modeled as a load-dependent current source. Since the RF voltage is constant and the current increases as the load resistance decreases, this load-dependent current source works opposite to the Tx suited for the load impedance (Z_{tx}) expressed in (6). A load-dependent voltage source, which has an exact duality with the load-dependent current source, can be introduced for the Tx of the WPT systems having multiple Rx's. It should have a constant RF current and RF voltage, which is determined by the Z_{tx}. As a result, the Tx can generate the appropriate power according to the variable power demand

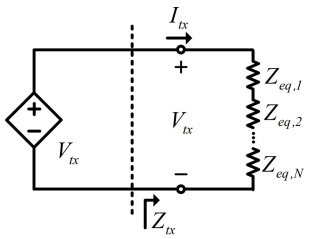

FIGURE 4. Simplified schematic diagram of the WPT Tx using the load-dependent voltage source.

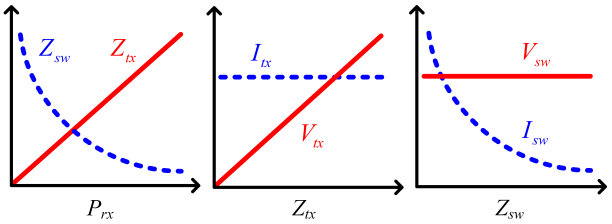

FIGURE 5. Relationship of voltages, currents, and impedances for the WPT Tx: (a) load impedances at the switch and Tx output, (b) voltage and current at the Tx output, and (c) voltage and current at the switch.

of the multiple Rx's without changing the supply voltage or without controlling any circuit component.

Fig. 4 shows a simplified schematic diagram of the WPT Tx using a load-dependent voltage source. If the current of the load-dependent voltage source is constant, the voltage V_{tx} should be proportional to Z_{tx} with a proportionality constant of α. Then, V_{tx} and P_{tx} can be expressed as follows.

$$V_{tx} = \alpha Z_{tx}, \tag{7}$$
$$P_{tx} = \alpha^2 Z_{tx}, \tag{8}$$

where α is independent to Z_{tx}. Z_{tx} is a pure real value. Since P_{DC} is proportional to V_{DC}^2 for Class-E PA, (4) can be rewritten as follows.

$$P_{tx} = P_{DC} = \beta V_{DC}^2 Z_{tx}, \tag{9}$$

where

$$\alpha^2 = \beta V_{DC}^2. \tag{10}$$

β is a constant and is independent to Z_{tx}.

Therefore, from (9), I_{DC}, I_{tx}, and V_{tx} can be represented using V_{DC} and Z_{tx} as:

$$I_{DC} = \beta V_{DC} Z_{tx}, \tag{11}$$
$$I_{tx} = \sqrt{\beta} V_{DC}, \tag{12}$$
$$V_{tx} = \sqrt{\beta} V_{DC} Z_{tx}. \tag{13}$$

Fig. 5 shows a relationship of voltages, currents, and impedances for the WPT Tx. If the PA operates as a load-dependent voltage source for Z_{tx}, P_{tx} can increase as Z_{tx} increases according to the increase in power demand of the Rx's (Fig. 5(a)). In this case, V_{tx} proportionally increases according to the increasing Z_{tx} while I_{tx} remains constant

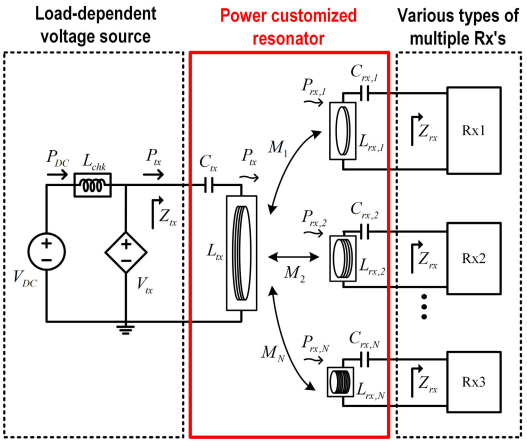

FIGURE 6. Schematic diagram of the proposed WPT system to charge various types of multiple Rx's.

(Fig. 5(b)). However, the switch of the PA basically becomes a load-dependent current source for the fundamental signal. Accordingly, P_{sw} is inversely proportional to Z_{sw} which is the load impedance at the switch plane. Therefore, as the power demand of the Rx increases, Z_{sw} should decrease, which leads to an increase in P_{sw} (Fig. 5(a)). For this case, I_{sw} increases as Z_{sw} decreases while V_{sw} is maintained (Fig. 5(c)). An appropriate load network is required to transform the load-dependent current source for Z_{sw} to the load-dependent voltage source for Z_{tx}. The load network and its design method for the load-dependent voltage source will be presented in section III-A.

B. PCR FOR CHARGING VARIOUS TYPES OF MULTIPLE RX'S

Fig. 6 shows a schematic diagram of the proposed WPT system to charge various types of multiple Rx's. The proposed WPT system consists of one Tx and N Rx's. The input impedances of the rectifiers for N Rx's are matched to the same reference impedance of Z_{rx}. To charge a single Rx, the Tx should generate the appropriate power for the Rx which could have different power demands. To charge multiple Rx's, including both homogeneous and heterogeneous configurations of the Rx's, the Tx should generate sufficient power to satisfy the total sum of the power demand from multiple Rx's. The power generated from the Tx should be distributed to the Rx's according to the power demand.

The mutual inductance of M_i between the Tx and i-th Rx coils can be expressed as follows.

$$M_i = k_i \sqrt{L_{tx} L_{rx,i}}, \tag{14}$$

where k_i is a coupling coefficient between the Tx and i-th Rx coils. L_{tx} and $L_{rx,i}$ are self-inductances of the Tx and the i-th Rx coils, respectively. Using (6) and (14), Z_{tx} can be derived using the parameters of the resonator as:

$$Z_{tx} = \frac{\omega_0^2 L_{tx}}{Z_{rx}} \sum_{i=1}^{N} k_i^2 L_{rx,i}. \tag{15}$$

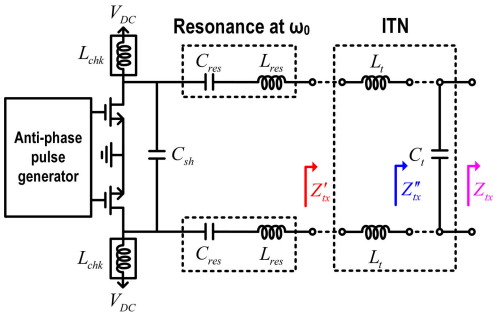

FIGURE 7. Schematic diagram of the load-dependent voltage source using a differential Class-E PA.

Using (12) and (15), P_{tx} can be derived as follows.

$$P_{tx} = \frac{\beta V_{DC}^2 \omega_0^2 L_{tx}}{Z_{rx}} \sum_{i=1}^{N} k_i^2 L_{rx,i}. \tag{16}$$

Then, $P_{rx,i}$, the received power of the i-th Rx, can be derived as follows.

$$P_{rx,i} = I_{tx}^2 Z_{eq,i} = \frac{\omega_0^2}{Z_{rx}} L_{tx} k_i^2 L_{rx,i} I_{tx}^2. \tag{17}$$

Using (12), (17) can be rewritten as:

$$P_{rx,i} = \frac{\beta V_{DC}^2 \omega_0^2}{Z_{rx}} L_{tx} k_i^2 L_{rx,i}. \tag{18}$$

As shown in (16) and (18), the output power of the Tx (P_{tx}) and the received power of the i-th Rx ($P_{rx,i}$) are derived as functions of the design parameters of the resonator, such as L_{tx}, $L_{rx,i}$, and k_i. Therefore, the design parameters of the proposed PCR can be easily determined using numerical adaptation based on the output power of the Tx, the power demand of each Rx, and various total power demands of various configurations of multiple Rx's. Additionally, practical conditions, such as a physical size of the device and the distance between the Tx and Rx coils, should be carefully considered. The design method of the proposed PCR based on the analysis above will be presented in Section III-C.

III. DESIGN OF THE WPT SYSTEM

The WPT system, including the load-dependent voltage source as a Tx, multiple Rx's, and the proposed PCR, was co-designed based on the results of the analysis in Section II.

A. LOAD-DEPENDENT VOLTAGE SOURCE

Fig. 7 shows a schematic diagram of the load-dependent voltage source using a differential Class-E PA. The differential PA has advantages in twice the output power and better even harmonic rejection characteristics compared to a single-ended PA with the same supply voltage. The load network of the Class-E PA consists of a shunt capacitor of C_{sh}, the series resonance networks using C_{res} and L_{res}, and the ITN. Z_{tx} and Z'_{tx} are the load impedances of the Class-E PA with and without ITN, respectively. Z''_{tx} is the load impedance of Class-E PA looking at C_t of the ITN.

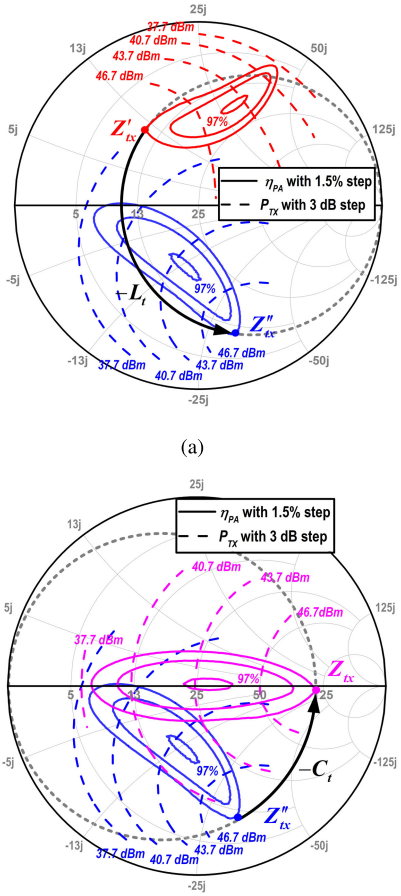

(a) (b)

FIGURE 8. Transformation of the output power and efficiency contours: (a) from Z'_{tx} to Z''_{tx}, (b) from Z''_{tx} to Z_{tx}.

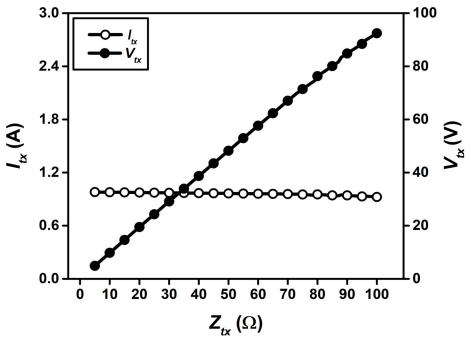

FIGURE 9. Simulated I_{tx} and V_{tx} according to Z_{tx} for the designed load-dependent voltage source.

The SPICE model of Fairchild's power MOSFET, FDMC86248, was used to design the load-dependent voltage source. The supply voltage of V_{DC} is 18 V. Fig. 8 shows the transformation of the power and efficiency contours for the impedances on the Smith chart using a load-pull simulation with steps of 3 dB and 1.5% for the power and efficiency, respectively. For Z'_{tx}, the high-efficiency area is located in the region that has a positive reactance, as shown

TABLE 1. Design parameters of the Rx's for three different mobile devices.

Rx type (Prototype)	Voltage (V)	Power (W)	Current (A)	Load (Ω)
Type-A (Laptop)	25	40	1.60	15.6
Type-B (Tablet)	15	20	1.33	11.3
Type-C (Cell phone)	12	10	0.83	14.5

in Fig. 8(a). However, if C_{tx} is in perfect resonance with the self-inductance of the Tx coil, the load impedance of the Tx, Z_{tx}, should have no reactance. Therefore, two conditions for the power and efficiency contours should be satisfied to realize a highly-efficient load-dependent voltage source using Class-E PA. First, the high-efficiency area in the contours should be located on the real axis of the Smith chart. Second, as the load impedance increases, the output power should increase with the same increasing rate.

The ITN should be designed to shift the power and efficiency contours to satisfy the two conditions above. Using the series inductor of L_t, the contours shift from the impedance plane of Z'_{tx} to that of the Z''_{tx} plane along with a constant resistance circle (Fig. 8(a)). This process can be formulated as follows.

$$Z''_{tx} = Z'_{tx} - j\omega L_t. \tag{19}$$

Using the shunt capacitor of C_t, the contours shift from the impedance plane of Z''_{tx} to that of Z_{tx} along with a constant conductance circle (Fig. 8(b)). It can be written as:

$$\frac{1}{Z_{tx}} = \frac{1}{Z''_{tx}} - j\omega C_t. \tag{20}$$

As shown in Fig. 8(b), the efficiency contours at the Z_{tx} plane are located well on the real axis using appropriate values of L_t and C_t. The highest efficiency area above 97% is located at around 30 Ω. In addition, as Z_{tx} increases on the real axis, the output power increases with a similar rate. Output power levels of 40.7, 43.7, and 46.7 dBm were obtained for Z_{tx}'s of 12.5, 25, and 50 Ω, respectively. Fig.9 shows the simulated I_{tx} and V_{tx} according to Z_{tx} for the designed load-dependent voltage source. According to the Z_{tx} from 5 to 100 Ω, I_{tx} remains almost constant at 0.96 A. V_{tx} increases with a constant slope of about 0.94, which is almost 1 and will be used to obtain α for the PCR design.

B. RX DESIGN USING A FULL-BRIDGE RECTIFIER

Three mobile devices, such as a laptop, tablet, and cell phone, are selected to design the three types of Rx's (type-A, -B, and -C). The load resistances for three different applications are estimated considering the power demand for each device and are presented in TABLE 1. For constant-current or constant-voltage charging, additional circuits, such as a dc-dc converter, are required after the Rx's.

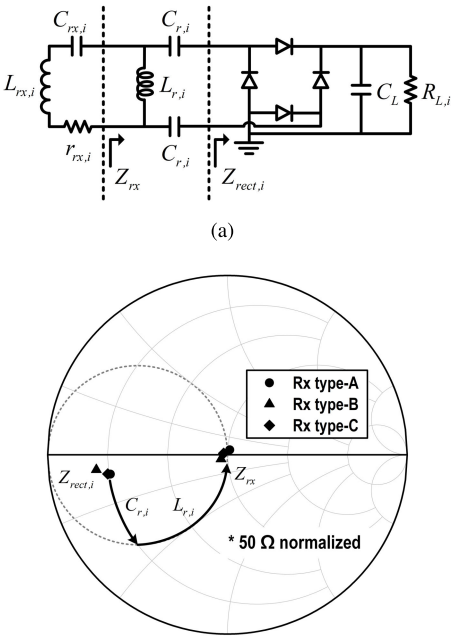

FIGURE 10. Design for three types of Rx's: (a) schematic diagram, (b) impedance matching trajectory.

The full-bridge rectifier was designed using four Schottky diodes, Diodes' DFLS240L. Fig. 10(a) shows a schematic diagram of the i-th Rx which could be one of three types. Fig. 10(b) is trajectory for the impedance matching on the Smith chart. $R_{L,i}$ is the load resistance of the rectifier in the i-th Rx, and C_L is a large shunt capacitor for the DC output voltage. $Z_{rect,i}$ is the input impedance of the rectifier in the i-th Rx. $C_{r,i}$ and $L_{r,i}$ are used to match the rectifier to have the given input impedance, $Z_{rect,i}$, of 50 W. For the Rx type-A, -B, and -C, the simulated $Z_{rect,i}$'s are 10.3-j3.9, 7.7-j2.8, and 9.8-j3.8, respectively.

C. POWER CUSTOMIZED RESONATOR DESIGN

The resonator for multiple Rx's should make the Tx sufficiently generate the output power and should distribute the power appropriately to multiple Rx's according to the power demand of each Rx. Using (16) and (18) in Section II, P_{tx} and $P_{rx,i}$ were derived using the parameters of the resonator. If the given or obtained values of the parameters, such as Ω_0 of $2\pi \cdot 6.78 \cdot 10^6$ rad/s, α of 0.94, V_{DC} of 18 V, and Z_{rx} of 50 Ω, are applied to (16) and (18), P_{tx} and $P_{rx,i}$ can be rewritten as:

$$P_{tx} = (3.41 \times 10^{13}) \cdot L_{tx} \sum_{i=1}^{N} k_i^2 L_{rx,i}, \tag{21}$$

$$P_{rx,i} = (3.41 \times 10^{13}) \cdot L_{tx} k_i^2 L_{rx,i}. \tag{22}$$

Since L_{tx} is common for all Rx's, $P_{rx,i}$ should be proportional to $k_i^2\ L_{rx,i}$. The following relationship can be derived using (22), and the parameters of three Rx's are shown in

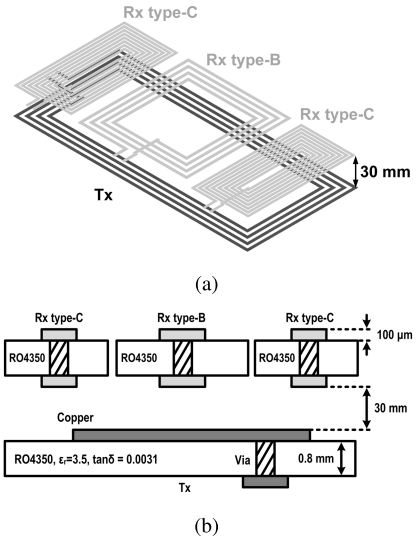

FIGURE 11. EM simulation setup for the PCR with one type-B Rx coil and two type-C Rx coils on top of the Tx coil: (a) 3-D view, (b) layer information.

TABLE 1.

$$k_1^2 L_{rx,1} : k_2^2 L_{rx,2} : k_3^2 L_{rx,3} = P_{rx,1} : P_{rx,2} : P_{rx,3} = 4 : 2 : 1. \tag{23}$$

Considering the physically allowable dimensions of the three types of Rx's, the PCR, including the Tx coil and three types of Rx coils, and distance between the Tx and Rx coils, should be designed using an EM simulation. The circuit parameters are extracted from the EM simulation results to check if they satisfy the relationship shown in (23). A few iterations may be required to accurately design the PCR that can exactly distribute the received power to multiple Rx's.

The dimensions of the Rx coils were determined to fit in the general sizes of the actual devices. The sizes of the Rx coils for types A, B, and C are set as 26 × 12, 11 × 12, and 6 × 12 cm^2, respectively. The size of the Tx coil was determined to be 26 × 12 cm^2 to be able to maximally charge one type-A, two type-B, or four type-C Rx's. The distance between the Tx and Rx coils is set to 30 mm to comply with the Alliance for Wireless Power (A4WP) standard. The coupling coefficient, k_i, is the ratio of the flux linked to the i-th Rx coil to the magnetic flux formed by the Tx coil. Therefore, k_i is mainly dependent on the dimension of the coil and the distance between the Tx and Rx coils. In addition, k_i does not significantly change, even if the number of turns of the coil has changed. In contrast, the number of turns can critically change the self-inductance, $L_{rx,i}$, of the coil.

The EM field simulation for the PCR was conducted using the Momentum in Keysight's Advanced Design System (ADS). Fig. 11 shows an example of the EM simulation setup using one Rx type-B and two Rx type-C coils on top of the Tx coil: (a) 3-D view and (b) layer information. Roger's RO4350B with a relative permittivity of 3.5 and a loss tangent of 0.0031 was used to implement the Tx and

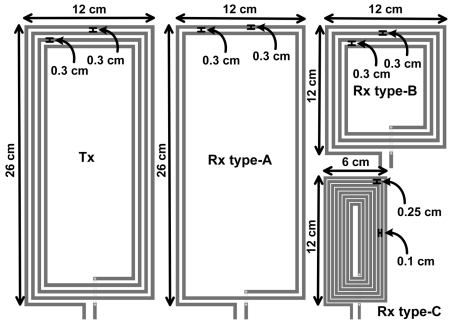

FIGURE 12. Dimensions of the designed coils for the Tx, Rx type-A, -B, and -C.

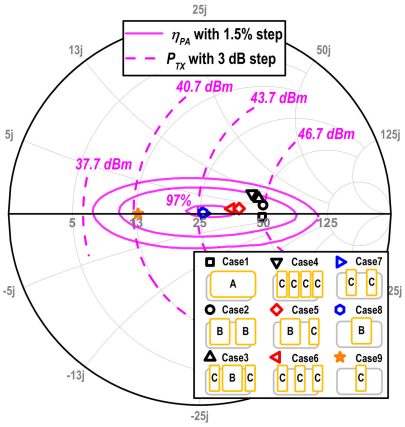

FIGURE 13. Simulated Z_{tx} with contours for the output power and efficiency of the PCR for various charging cases.

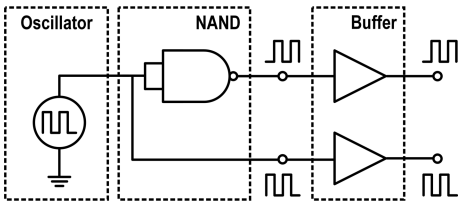

FIGURE 14. Block diagram of the anti-phase pulse generator as the PA driver.

Rx coils. If k_i for the i-th Rx coil is estimated using the EM simulation, the values of L_{tx} and $L_{rx,i}$ can be determined to satisfy the conditions in (21) and (22). Among the value sets of L_{tx} and $L_{rx,i}$, the most appropriate set should be selected while considering the size of the resonator. The values of the circuit parameters for three Rx types, such as k_i, L_{tx}, $L_{rx,i}$, r_{tx}, and $r_{rx,i}$, are summarized in TABLE 2. r_{tx} and $r_{rx,i}$ are the equivalent series resistances of the Tx and i-th Rx coils, respectively.

Fig. 12 shows the dimensions of the coils for the Tx and type-A, type-B, and type-C Rx's that are designed to have the optimized circuit parameters for power distribution to multiple Rx's. The pattern width and spacing of the Tx and type-A and type-B Rx coils are 0.3 cm, while those of the type-C Rx coil is 0.25 and 0.1 cm, respectively. In order to realize L_{tx} and $L_{rx,i}$ into the dimensions of the coils, the number of turns of the Tx and type-A, type-B, and type-C Rx's are

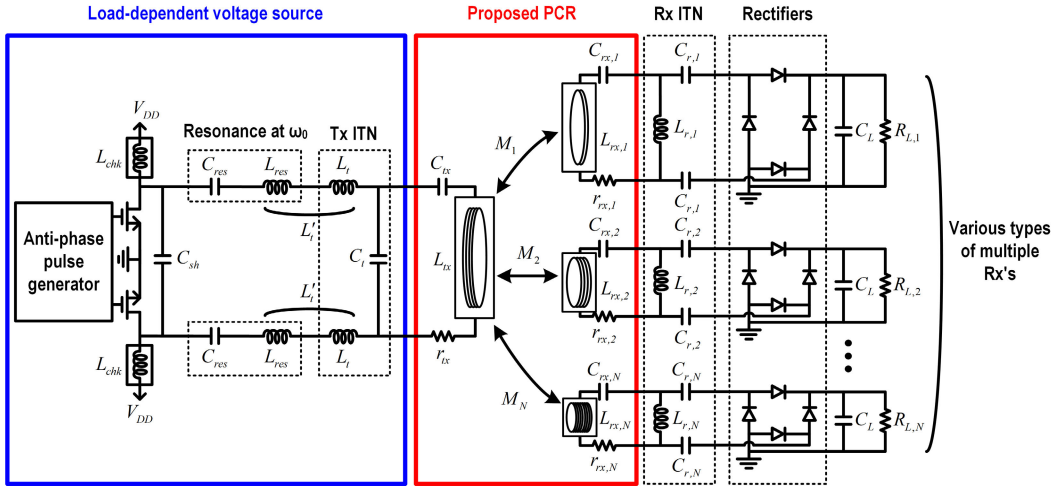

FIGURE 15. Schematic diagram of the proposed WPT system to charge various types of the multiple Rx's.

TABLE 2. Circuit parameters of the PCR extracted from the EM simulation Results.

Resonator	k_i	L_{tx} or $L_{rx,i}$ (μH)	r_{tx} or $r_{rx,i}$ (Ω)
Tx	-	5.77	0.989
Rx Type-A	0.34	1.98	0.474
Rx Type-B	0.21	2.67	0.496
Rx Type-C	0.12	4.25	1.381

TABLE 3. Configurations of the PCR for various charging cases.

Charging case	Rx configuration	PCR
1	One Rx type-A	
2	Two Rx type-B	
3	One Rx type-B, two Rx type-C	
4	Four Rx type-C	
5	One Rx type-B, one Rx type-C	
6	Three Rx type-C	
7	Two Rx type-C	
8	One Rx type-B	
9	One Rx type-C	

optimized to be 4, 2, 4, and 8, respectively. The experiments were carried out for the nine charging cases selected that include homogeneous and heterogeneous configurations of the multiple Rx's, as shown in TABLE 3.

Fig. 13 shows the simulated Z_{tx}'s with the contours of output power and efficiency for the selected charging cases. For cases 1 to 4, the total power demand for the Rx is about 40 W. For these cases, Z_{tx}'s are formed near 50 Ω where the output power of the load-dependent voltage source is 46.7 dBm (46.8 W). For cases 5 and 6, the total power demand of the Rx is about 30 W. For these cases, Z_{tx}'s are formed at around 37.5 Ω where the output power of the Tx is 45.5 dBm (35.1 W). For cases 7 and 8, the total power demand of Rx is about 20 W. The Z_{tx}'s are formed at near 25 Ω where the output power is 43.7 dBm (23.4 W). For case 9, the power demand from Rx is about 10 W. Z_{tx} becomes near 12.5 Ω, where the output power of the Tx is 40.7 dBm (11.7 W). Considering the loss of the PCR and the full-bridge rectifier, the parameters of the PCR were determined to have slightly larger output levels from the Tx than the power demand from the Rx's for the charging cases.

The cross coupling between two adjacent Rx coils may cause an error in the Z_{tx}'s. Due to the mutual inductance between two adjacent Rx coils, though, it should be relatively small compare to that with the Tx coil, and the simulated Z_{tx}'s, especially for cases 2 to 4, have small imaginary parts. However, as shown in Fig. 12, these imaginary parts are not so significant to have noticeable effect on the output power and efficiency. The effect of the cross coupling between the two Rx coils was comprehensively analyzed in [6]. Misalignment of the resonant coils can change the mutual inductance between the Tx and Rx coils, which results

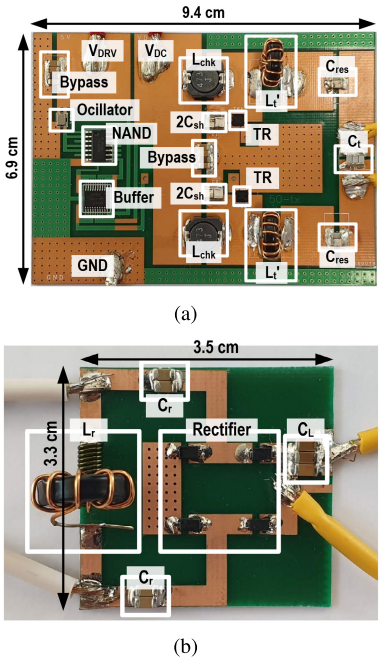

FIGURE 16. Photographs of the implemented WPT system: (a) Tx including the load-dependent voltage source and the PA driver, (b) Rx type-A.

in the load impedance variation for the Tx [7], [9]. However, in this work, it was assumed that the multiple Rx's were well-aligned.

D. ANTI-PHASE PULSE GENERATOR FOR THE PA DRIVER

A simple anti-phase pulse generator was designed to drive the differential Class-E PA. Two pulse output signals of the generator have a phase difference of 180°. Fig. 14 shows the block diagram of the anti-phase pulse generator for the PA driver. A crystal oscillator generates the pulse with an oscillation frequency of Ω_0. The NAND gate inverts the signal of the oscillator. After that, the current buffer provides a sufficient current to the gates of the PA.

IV. IMPLEMENTATION AND EXPERIMENTAL RESULTS

Fig. 15 shows a schematic diagram of the proposed WPT system to charge multiple Rx's of various types. Two series inductors of L_{res} and L_t are merged into an inductor of L_t'. The load-dependent voltage source was designed using a differential Class-E PA with a simple L-C ITN for the Tx. An anti-phase pulse generator was used to drive the load-dependent voltage source. Three types of Rx type-A, −B, and −C, with different power demands for their respective applications were designed and used for the experiment with the proposed PCR and Tx based on the load-dependent voltage source. A full-bridge structure is adopted for the rectifier, and the input impedance is transformed into the reference impedance using the Rx ITN. The PCR was designed for the Tx to generate the required power and to appropriately distribute the transmitted power to each Rx according to its power demand.

TABLE 4. Component values and part numbers for the designed WPT system.

System block	Component	Part number or values
Tx	Transistor	FDMC86248
	C_{res}	1100 pF
	Lt_t	1.0 μH
	C_t	690 pF
	C_{sh}	250 pF
	L_{chk}	47 μH
	C_{tx}	95 pF
Rx (common)	C_L	40 μF
	Diode	DFLS240
Rx type-A	$L_{r,i}$	0.582 μH
	$C_{r,i}$	3200 pF
	$C_{rx,i}$	280 pF
Rx type-B	$L_{r,i}$	0.5 μH
	$C_{r,i}$	3200 pF
	$C_{rx,i}$	200 pF
Rx type-C	$L_{r,i}$	0.568 μH
	$C_{r,i}$	3000 pF
	$C_{rx,i}$	129 pF
Anti-phase pulse generator	Oscillator	SG-210STF
	NAND	74AC00SCX
	Buffer	SN74AHC541PWR

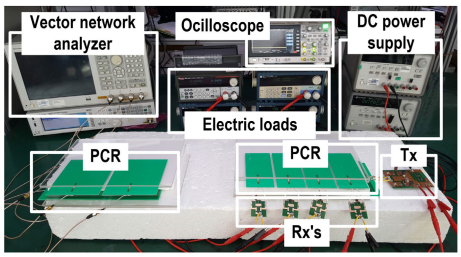

FIGURE 17. Photograph of the measurement setup for the proposed WPT system.

Fig. 16 shows photographs of the circuit blocks implemented for the proposed WPT system consisting of (a) Tx including the load-dependent voltage source and the PA driver, (b) type-A Rx. The sizes of the Tx and type-A Rx without the PCR are $9.4 \times 6.9\ cm^2$ and $3.5 \times 3.3\ cm^2$, respectively. A substrate based on FR4 with a thickness of 40 mil was used to implement both the Tx and Rx circuits. The values or part numbers of the components for the designed WPT system are listed in TABLE 4.

Fig. 17 shows a photograph of the measurement setup for the proposed WPT. DC voltages of 18 V and 5 V are applied to the Class-E PA and the input gate driver, respectively. Electric loads (Keithley's 2380 and Maynuo's M9712) are used to provide different load resistances to multiple Rx's and to measure the received DC power. The waveforms were probed using an oscilloscope (Keysight's DSOX1120G), and the series resonance frequency is measured using a vector network analyzer (Keysight's E5071B).

TABLE 5. Performance comparison with previous works of mid-range wireless power transfer system.

Ref.	Freq. (MHz)	Topology			Rx's configuration (# of Rx's)	Charging distance (cm)	Tunable or adaptive	Performance		Fetures
		PA	Resonator	Rectifier				$P_{rx,max}$ (W)	$\eta_{sys,max}$ (%)	
[16]	6.78	Class-E	[a]Conv.	Class-E	Single (1)	2-6	No	[*]27.0	[*]81.0	ITN for charging distance variation
[17]	13.56	Class-E	Conv.	[†]N/A	Single (1)	0-120	Capacitor matrix	1	88.0	High-efficiency tracking for charging distance variation
[18]	0.3	Class-D	Conv.	Full-bridge	Single (1)	5.5-10	Feedback	10	76.0	Rx duty-cycle control for coupling coefficient variation
[19]	6.78	Class-E	Conv.	Full-bridge	Homogeneous (3)	2	Feedback	20	71.7	Adaptive tracking for maximum efficiency point
[20]	6.78	Class-E	Conv.	Full-bridge	Homogeneous (6)	3	No	[*]27.8	[*]74.7	Equalization process of six battery voltages
[21]	6.78	Class-E	Conv.	Full-bridge	Single (1), Homogeneous (2, 3, 4), Heterogeneous (2, 3)	3-5	[b]SSC	39.7	81.4	Reconfigurable PA for various charging cases
This work	6.78	Class-E	PCR	Full-bridge	Single (1), Homogeneous (2, 3, 4), Heterogeneous (2, 3)	3	No	45.7	85.5	Power customized resonator for various charging cases

[*]Graphically estimated, [†]N/A: not available.
[a]Conventional, [b]Susceptance switching circuit.

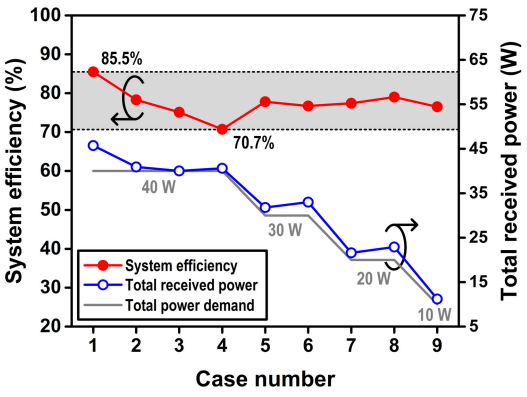

FIGURE 18. Measured system efficiency and total received DC power for cases 1 to 9.

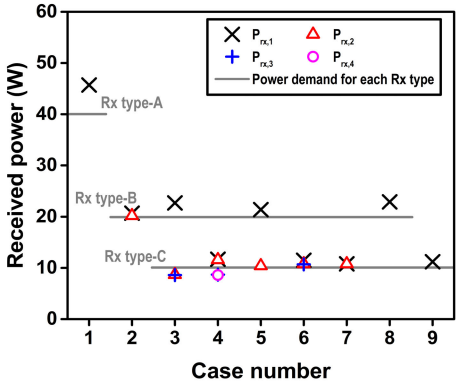

FIGURE 19. Measured received DC power of each Rx for charging cases 1 to 9.

Fig. 18 shows the measured system efficiency and the total DC power received for cases 1 to 9. The system efficiency was calculated by the ratio of the sum of the measured DC power at the Rx's and the measured DC power consumption of the all Tx circuits including the load-dependent voltage source and the PA driver. The system efficiency remained above 70.7% and the highest efficiency of 85.5% was obtained for the charging case 1. The total received power levels measured for all the charging cases are slightly higher than the power demand for each case, as shown in Fig. 18. Therefore, the proposed PCR was proven to be able to provide the load impedance for the Tx to generate sufficient power.

Fig. 19 shows the measured received DC power of each Rx for the charging cases of from 1 to 9. As shown, the measured received DC power is very close to the power demand of each Rx. The power demands of the type-A, -B, and -C Rx's are 40, 20, and 10 W, respectively. Therefore, the proposed PCR was also proven to distribute the total received power to each Rx according to its power demand for any different

configurations of multiple Rx's. Due to the cross-coupling effect between the two adjacent Rx's, the received power levels for two type-C Rx's in charging cases 3 and 4 are just a little lower with 8.7 and 8.6 W, respectively, than their power demands. Measured performances were compared to those of the previous works in TABLE 5.

V. CONCLUSION

This paper presented a high-efficiency WPT system to charge multiple Rx's of various types based on a combination of the proposed PCR and load-dependent voltage source. The equivalent circuit parameters of the resonator for the multiple Rx's were analyzed and represented using the transmitted power and received power of each Rx. Based on the analysis, the PCR that allows the Tx to generate sufficient output power and distributes the received power to each Rx according to its power demand was proposed. Using the proposed PCR, each Rx matched by the reference impedance of any configurations using the multiple Rx's can receive sufficient power for the power demand.

In combination with the PCR, a load-dependent voltage source was proposed to generate various levels of required power with a high-efficiency. Over a wide impedance range, the load-dependent voltage source using a differential class-E PA was successfully designed with a simple ITN and without complex reconfigurable circuits.

The WPT system, including the Tx based on the load-dependent voltage source, the PCR, and three types of Rx's, was designed and implemented. The implemented system was verified for nine selected charging cases through experiments. A very high system efficiency from 70.7 to 85.5% were experimentally achieved with a received power for each Rx ranging from 8.6 to 45.7 W. In addition, it was experimentally verified that each Rx can receive sufficient power according to its power demand from any of the multiple Rx configurations using the proposed PCR.

REFERENCES

[1] A. Kurs, R. Moffatt, and M. Soljačić, "Simultaneous mid-range power transfer to multiple devices," *Appl. Phys. Lett.*, vol. 96, no. 4, Jan. 2010, Art. no. 044102.

[2] D. Ahn and S. Hong, "Effect of coupling between multiple transmitters or multiple receivers on wireless power transfer," *IEEE Trans. Ind. Electron.*, vol. 60, no. 7, pp. 2602–2613, Jul. 2013.

[3] H. Hwang, J. Moon, B. Lee, C.-H. Jeong, and S.-W. Kim, "An analysis of magnetic resonance coupling effects on wireless power transfer by coil inductance and placement," *IEEE Trans. Consum. Electron.*, vol. 60, no. 2, pp. 203–209, May 2014.

[4] K. E. Koh, T. C. Beh, T. Imura, and Y. Hori, "Impedance matching and power division using impedance inverter for wireless power transfer via magnetic resonant coupling," *IEEE Trans. Ind. Appl.*, vol. 50, no. 3, pp. 2061–2070, May 2014.

[5] M. Fu, T. Zhang, C. Ma, and X. Zhu, "Efficiency and optimal loads analysis for multiple-receiver wireless power transfer systems," *IEEE Trans. Microw. Theory Techn.*, vol. 63, no. 3, pp. 801–812, Mar. 2015.

[6] M. Fu, T. Zhang, X. Zhu, P. C.-K. Luk, and C. Ma, "Compensation of cross coupling in multiple-receiver wireless power transfer systems," *IEEE Trans. Ind. Informat.*, vol. 12, no. 2, pp. 474–482, Apr. 2016.

[7] S. Aldhaher, P. C.-K. Luk, and J. F. Whidborne, "Electronic tuning of misaligned coils in wireless power transfer systems," *IEEE Trans. Power Electron.*, vol. 29, no. 11, pp. 5975–5982, Nov. 2014.

[8] J. Choi, J. Xu, R. Makhoul, and J. M. R. Davila, "Implementing an impedance compression network to compensate for misalignments in a wireless power transfer system," *IEEE Trans. Power Electron.*, vol. 34, no. 5, pp. 4173–4184, May 2019.

[9] H. Qiu, T. Sakurai, and M. Takamiya, "Digital transmitter coil for wireless power transfer robust against variation of distance and lateral misalignment," *IEEE Trans. Microw. Theory Techn.*, vol. 68, no. 9, pp. 4031–4039, Sep. 2020.

[10] M. Liu, M. Fu, and C. Ma, "Parameter design for a 6.78-MHz wireless power transfer system based on analytical derivation of class E current-driven rectifier," *IEEE Trans. Power Electron.*, vol. 31, no. 6, pp. 4280–4291, Jun. 2016.

[11] S. Liu, M. Liu, S. Han, X. Zhu, and C. Ma, "Tunable class E^2 DC–DC converter with high efficiency and stable output power for 6.78-MHz wireless power transfer," *IEEE Trans. Power Electron.*, vol. 33, no. 8, pp. 6877–6886, Aug. 2018.

[12] Y.-J. Kim, D. Ha, W. J. Chappell, and P. P. Irazoqui, "Selective wireless power transfer for smart power distribution in a miniature-sized multiple-receiver system," *IEEE Trans. Ind. Electron.*, vol. 63, no. 3, pp. 1853–1862, Mar. 2016.

[13] J. Kim, D.-H. Kim, and Y.-J. Park, "Free-positioning wireless power transfer to multiple devices using a planar transmitting coil and switchable impedance matching networks," *IEEE Trans. Microw. Theory Techn.*, vol. 64, no. 11, pp. 3714–3722, Nov. 2016.

[14] W. Zhong and S. Y. R. Hui, "Maximum energy efficiency operation of series-series resonant wireless power transfer systems using on-off keying modulation," *IEEE Trans. Power Electron.*, vol. 33, no. 4, pp. 3595–3603, Apr. 2018.

[15] K. Xie, A. Huang, L. Chen, S. Guo, and H. Zhang, "Half-cycle resonance tracking for inductively coupled wireless power transmission system," *IEEE Trans. Power Electron.*, vol. 33, no. 3, pp. 2668–2679, Mar. 2018.

[16] S. Liu, M. Liu, S. Yang, C. Ma, and X. Zhu, "A novel design methodology for high-efficiency current-mode and voltage-mode class-E power amplifiers in wireless power transfer systems," *IEEE Trans. Power Electron.*, vol. 32, no. 6, pp. 4514–4523, Jun. 2017.

[17] Y. Lim, H. Tang, S. Lim, and J. Park, "An adaptive impedance-matching network based on a novel capacitor matrix for wireless power transfer," *IEEE Trans. Power Electron.*, vol. 29, no. 8, pp. 4403–4413, Aug. 2014.

[18] D. Ahn, S. Kim, J. Moon, and I.-K. Cho, "Wireless power transfer with automatic feedback control of load resistance transformation," *IEEE Trans. Power Electron.*, vol. 31, no. 11, pp. 7876–7886, Nov. 2016.

[19] M. Fu, H. Yin, and C. Ma, "Megahertz multiple-receiver wireless power transfer systems with power flow management and maximum efficiency point tracking," *IEEE Trans. Microw. Theory Techn.*, vol. 65, no. 11, pp. 4285–4293, Nov. 2017.

[20] M. Liu, M. Fu, Y. Wang, and C. Ma, "Battery cell equalization via megahertz multiple-receiver wireless power transfer," *IEEE Trans. Power Electron.*, vol. 33, no. 5, pp. 4135–4144, May 2018.

[21] H. Oh, W. Lee, H. Koo, J. Bae, K. Hwang, K. Lee, and Y. Yang, "6.78 MHz wireless power transmitter based on a reconfigurable class-E power amplifier for multiple device charging," *IEEE Trans. Power Electron.*, vol. 35, no. 6, pp. 5907–5917, Jun. 2020.

[22] L. Jiang and D. Costinett, "A high-efficiency GaN-based single-stage 6.78 MHz transmitter for wireless power transfer applications," *IEEE Trans. Power Electron.*, vol. 34, no. 8, pp. 7677–7692, Aug. 2019.

[23] Y. Li, J. Hu, X. Li, and K.-W.-E. Cheng, "A flexible load-independent multi-output wireless power transfer system based on cascaded double T-resonant circuits: Analysis, design and experimental verification," *IEEE Trans. Circuits Syst. I, Reg. Papers*, vol. 66, no. 7, pp. 2803–2812, Jul. 2019.

[24] Y. Li, K. Huo, Q. Li, X. Liu, S. Jiang, J. Liu, and X. Ni, "A novel method of wireless power transfer identification and resonance decoupling based on frequency hopping communication," *IEEE Access*, vol. 7, pp. 161201–161210, 2019.

[25] S.-J. Jeon and D.-W. Seo, "Capacitance tuning method for maximum output power in multiple-transmitter wireless power transfer system," *IEEE Access*, vol. 8, pp. 181674–181682, 2020.

[26] M. Wagih, A. Komolafe, and B. Zaghari, "Dual-receiver wearable 6.78 MHz resonant inductive wireless power transfer glove using embroidered textile coils," *IEEE Access*, vol. 8, pp. 24630–24642, 2020.

[27] M. Liu and M. Chen, "Dual-band wireless power transfer with reactance steering network and reconfigurable receivers," *IEEE Trans. Power Electron.*, vol. 35, no. 1, pp. 496–507, Jan. 2018.

[28] C. H. Yeh, Y. T. Lin, C. C. Kuo, C. J. Huang, C. Y. Xie, S. F. Lu, W. H. Yang, K. H. Chen, K. C. Liu, and Y. H. Lin, "A 70 W and 90% GaN-based class-E wireless power-transfer system with automatic-matching-point-search control for zero-voltage switching and zero-voltage-derivative switching," in *IEEE Int. Solid-State Circuits Conf. (ISSCC) Dig. Tech. Papers*, San Francisco, CA, USA, 2018, pp. 138–140.
[29] X. Dai, X. Li, Y. Li, and A. P. Hu, "Maximum efficiency tracking for wireless power transfer systems with dynamic coupling coefficient estimation," *IEEE Trans. Power Electron.*, vol. 33, no. 6, pp. 5005–5015, Jun. 2018.
[30] S. Huh and D. Ahn, "Two-transmitter wireless power transfer with optimal activation and current selection of transmitters," *IEEE Trans. Power Electron.*, vol. 33, no. 6, pp. 4957–4967, Jun. 2018.
[31] H. Li, J. Fang, S. Chen, K. Wang, and Y. Tang, "Pulse density modulation for maximum efficiency point tracking of wireless power transfer systems," *IEEE Trans. Power Electron.*, vol. 33, no. 6, pp. 5492–5501, Jun. 2018.
[32] W. Zhong and S. Y. Hui, "Reconfigurable wireless power transfer systems with high energy efficiency over wide load range," *IEEE Trans. Power Electron.*, vol. 33, no. 7, pp. 6379–6390, Jul. 2018.
[33] M. Acar, A. J. Annema, and B. Nauta, "Analytical design equations for class-E power amplifiers," *IEEE Trans. Circuits Syst. I, Reg. Papers*, vol. 54, no. 12, pp. 2706–2717, Dec. 2007.
[34] J. Y. Hasani and M. Kamarei, "Analysis and optimum design of class E RF power amplifier," *IEEE Trans. Circuits Syst. I, Reg. Papers*, vol. 55, no. 6, pp. 1759–1768, Jul. 2008.

HANSIK OH was born in Seoul, South Korea, in 1991. He received the B.S. degree from the Department of Electronic and Electrical Engineering, Sungkyunkwan University, Suwon, South Korea, in 2016, where he is currently pursuing the Ph.D. degree with the Department of Electrical and Computer Engineering.

His current research interests include the design of RF power amplifiers, RF integrated circuits, analog integrated circuits, efficiency enhancement techniques, and linearization techniques.

SUNGJAE OH was born in Gwangju, South Korea, in 1992. He received the B.S. degree from the Department of Electronic and Electrical Engineering, Sungkyunkwan University, Suwon, South Korea, in 2015. He is currently pursuing the Ph.D. degree with the Department of Electrical and Computer Engineering.

His current research interests include the design of RF/mm-wave power amplifiers, analog integrated circuits, efficiency enhancement, broadband, and linearization techniques.

HYUNGMO KOO was born in Seoul, South Korea, in 1992. He received the B.S. degree from the Department of Electronic and Electrical Engineering, Sungkyunkwan University, Suwon, South Korea, in 2016. He is currently pursuing the Ph.D. degree with the Department of Electrical and Computer Engineering.

His current research interests include the design of RF power amplifiers, efficiency enhancement techniques, transceiver arrays, microwave power transmission, and passive circuits optimizations.

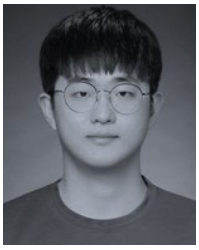

WOOJIN CHOI was born in Kyunggi-do, South Korea, in 1993. He received the B.S. degree from the Department of Electronic and Electrical Engineering, Sungkyunkwan University, Suwon, South Korea, in 2016. He is currently pursuing the Ph.D. degree with the Department of Electrical and Computer Engineering.

His current research interests include the design of RF/mm-wave power amplifiers, broadband techniques, and mm-wave integration circuits.

JAEKYUNG SHIN was born in Seoul, South Korea, in 1993. He received the B.S. degree from the Department of Electronic and Electrical Engineering, Korea Aerospace University, Goyang, South Korea, in 2018. He is currently pursuing the Ph.D. degree with the Department of Electrical and Computer Engineering, Sungkyunkwan University, Suwon, South Korea.

His current research interests include the design of RF/mm-wave power amplifiers, efficiency enhancement techniques, broadband techniques, and microwave power transmission.

KEUM CHEOL HWANG (Senior Member, IEEE) received the B.S. degree in electronics engineering from Pusan National University, Busan, South Korea, in 2001, and the M.S. and Ph.D. degrees in electrical and electronic engineering from the Korea Advanced Institute of Science and Technology (KAIST), Daejeon, South Korea, in 2003 and 2006, respectively. From 2006 to 2008, he was a Senior Research Engineer with Samsung Thales, Yongin, South Korea, where he was involved with the development of various antennas, including multiband fractal antennas for communication systems and Cassegrain reflector antenna and slotted waveguide arrays for tracking radars. He was an Associate Professor with the Division of Electronics and Electrical Engineering, Dongguk University, Seoul, South Korea, from 2008 to 2014. He joined the Department of Electronic and Electrical Engineering, Sungkyunkwan University, Suwon, South Korea, in 2015, where he is currently an Associate Professor. His research interests include advanced electromagnetic scattering and radiation theory and applications, design of multi-band/broadband antennas and radar antennas, and optimization algorithms for electromagnetic applications. He is a Life Member of KIEES and a Member of IEICE.

KANG-YOON LEE (Senior Member, IEEE) received the B.S., M.S., and Ph.D. degrees from the School of Electrical Engineering, Seoul National University, Seoul, South Korea, in 1996, 1998, and 2003, respectively. From 2003 to 2005, he was with GCT Semiconductor Inc., San Jose, CA, USA, where he was a Manager of the Analog Division and worked on the design of CMOS frequency synthesizer for CDMA/PCS/PDC and single-chip CMOS RF chip sets for W-CDMA, WLAN, and PHS. From 2005 to 2011, he was an Associate Professor with the Department of Electronics Engineering, Konkuk University. Since 2012, he has been with the College of Information and Communication Engineering, Sungkyunkwan University, Seoul, where he is currently an Associate Professor. His research interests include implementation of power integrated circuits, CMOS RF transceiver, analog integrated circuits, and analog/digital mixed-mode VLSI systems design.

YOUNGOO YANG (Senior Member, IEEE) was born in Hamyang, South Korea, in 1969. He received the Ph.D. degree in electrical and electronic engineering from the Pohang University of Science and Technology, Pohang, South Korea, in 2002.

From 2002 to 2005, he was with Skyworks Solutions, Inc., Newbury Park, CA, USA, where he designed power amplifiers for various cellular handsets. Since 2005, he has been with the School of Information and Communication Engineering, Sungkyunkwan University, Suwon, South Korea, where he is currently a Professor. His current research interests include RF/mm-wave power amplifiers, RF transmitters, and dc-dc converters.